Materials Today: Proceedings xxx (xxxx) xxx

Contents lists available at ScienceDirect

Materials Today: Proceedings

journal homepage: www.elsevier.com/locate/matpr

Modelling and experimental validation of TIG welding of INCONEL 718

S. Tamil Prabakaran [a,*], P. Sakthivel [d], Mohanraj Shanmugam [b], S. Satish [c], M. Muniyappan [d], V.S. Shaisundaram [e]

[a] Department of Mechanical Engineering, Government College of Engineering, Bargur, Tamilnadu, India
[b] Department of Materials Engineering and Nanotechnology, Politecnico di Milano, Milan, Italy
[c] Department of Automobile Engineering, Kumaraguru College of Technology, Coimbatore, India
[d] Department of Automobile Engineering, Easwari Engineering College, Chennai, India
[e] Department of Automobile Engineering, Vels Institute of Science Technology and Advanced Studies, Chennai, India

ARTICLE INFO

Article history:
Received 26 June 2020
Accepted 21 July 2020
Available online xxxx

Keywords:
TIG
Simulation
Welding
Deformations
Recrystallization

ABSTRACT

The overall aim behind the work presented in this thesis is to gain and apply an understanding of the coupled mechanical and metallurgical effects of TIG welding of nickel-base super alloy (IN718) by using experimentally validated finite element model, which employed for identify the location and size of recrystallized zone (HAZ) and hot cracking susceptible zone in HAZ.

- To develop an efficient and reliable Finite Element Model of TIG welding moving heat source and proper validation based on the experimental measurements.
- To experimental validation of thermal cycle predicted by FE model and study the data acquisition (DAQ) process and effectiveness of thermocouple.
- To analyze the thermal stress distribution pattern, FZ size and HAZ size by using finite element model.
- To investigate the susceptibility of HAZ hot cracking in INCONEL 718 weldment using FEM solutions.

Selection and peer-review under responsibility of the scientific committee of the International Conference on Newer Trends and Innovation in Mechanical Engineering: Materials Science.

1. Introduction

The most important reason for development model is the industrial need to improve productivity, reliability and quality of products and to have better understanding of the influence of different process parameters. The application numerical modeling lies in determining the evolution of metallurgical changes, and stresses to predict, for example, deformations, recrystallization, and susceptibility to HAZ hot cracking. SYSWELD simulation tool can be used to investigation of weldment.

Welding techniques are one of the most important and most often used methods for joining pieces in industry.

1.1. Heat source modeling

Modeling the welding process can be a tedious and nontrivial task due to the complex nature of the process, which involves several physical phenomena [1–3]. A fully detailed process model would need to include: accurate temperature history input or calculation (heat flux and boundary conditions), temperature-dependent material properties, addition of filler material (if any), mechanical effects such as distortion and clamping (if any), metallurgical transformations during heating and cooling phases, melt pool phenomena such as fluid flow and electromagnetic forces, chemical interaction with shielding gases etc. In order to reduce the demands of modeling such a complicated process, some simplifications are necessary [4–7].

Heat should be distributed throughout top surface and be distributed throughout the depth of the molten zone to reflect more accurately the digging action of the arc. A non-axisymmetric three-dimensional heat source model was proposed, taking the form of a 'double ellipsoid'. This model is more accurate, based on molten zone observations, and more flexible than its predecessors [8–11]

1.2. Material

IN718 is often used in critical high temperature creep resistant applications up to 650 °C [6]. One example of application within the aerospace industry is the gas turbine engine, where IN718 is

* Corresponding author.
E-mail address: tamilprabakarans@gmail.com (S. Tamil Prabakaran).

https://doi.org/10.1016/j.matpr.2020.07.482
2214-7853/
Selection and peer-review under responsibility of the scientific committee of the International Conference on Newer Trends and Innovation in Mechanical Engineering: Materials Science.

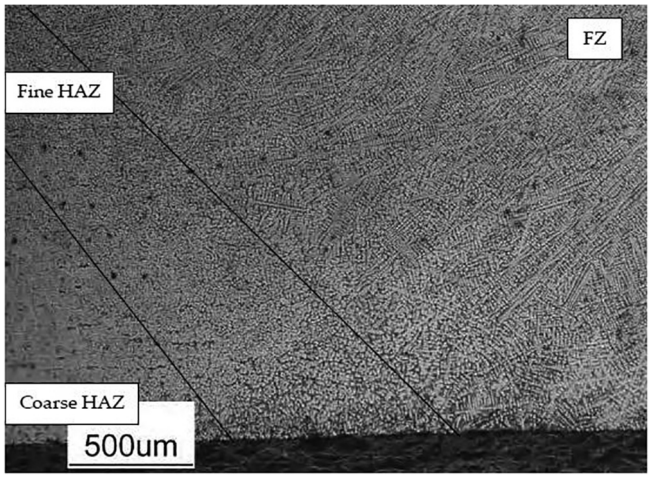

Fig. 1.1. IN718 weld microstructural zones FZ Fine HAZ Coarse HAZ.

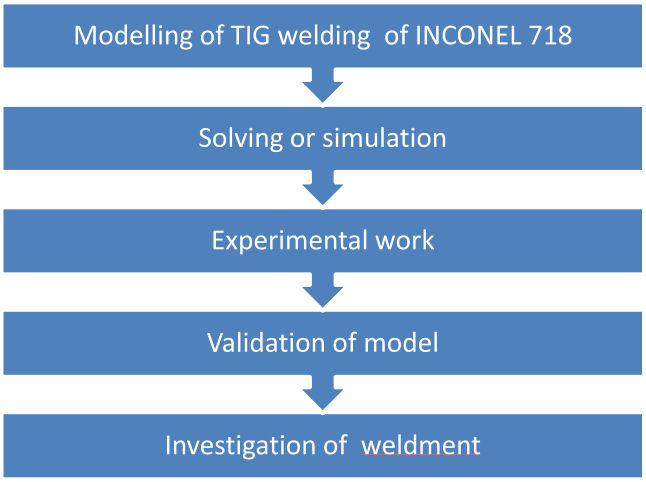

Fig. 2.1. Flow chart Methodology.

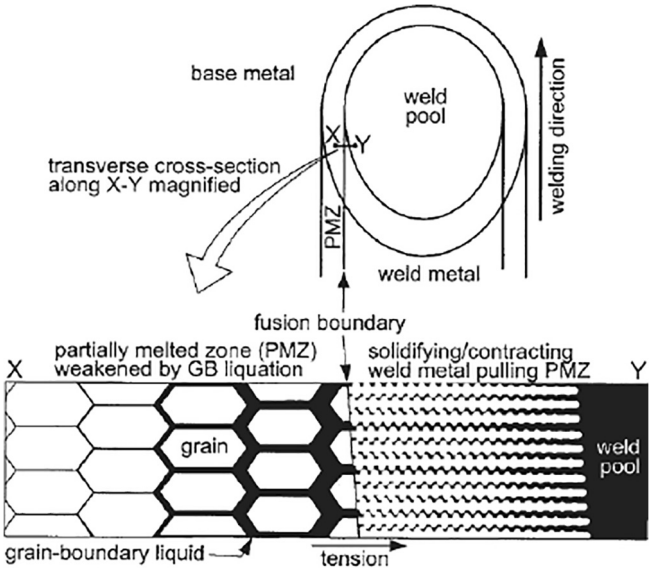

Fig. 1.2. Grain boundary liquation.

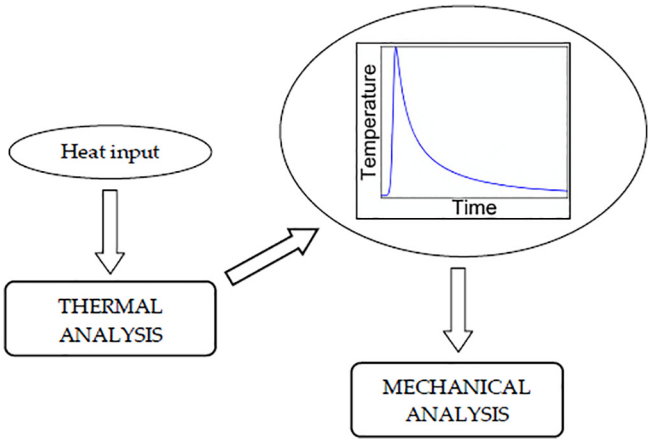

Fig. 2.2. Sequential coupling of the thermal and mechanical analyses.

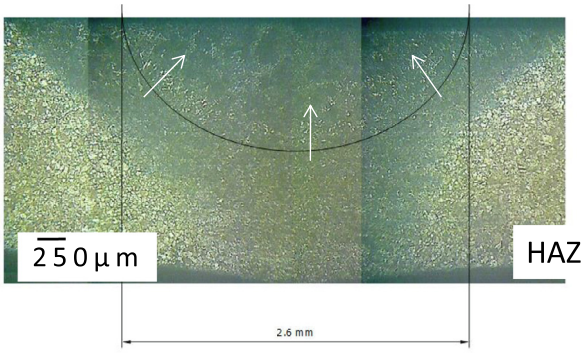

Fig. 2.3. Microstructure of weld pool profile - Transverse view (50X).

used for turbine disc forgings and shell structures such as the combustor [12–15]. Hence, it is essential to develop techniques to predict the mechanical and metallurgical effects of the welding process such as residual stress, recrystallisation (HAZ size and shape) and susceptibility of cracking.

1.2.1. The heat-affected zone (HAZ)

In the region directly adjacent to the fusion zone (FZ) exists base metal that undergoes a severe thermal cycle without melting. As a result, the microstructure and properties of this heat-affected zone (HAZ) change undesirably [16–19]. The HAZ can be divided into a number of subzones, the total number and type depends on the material being welded. Each subzone refers to a different type of microstructure. Common changes in microstructure are recrystallisation and grain growth. In IN718 welds, there are two HAZ regions: one coarse-grained and one fine-grained (Fig. 1.1). Grain growth is less pronounced in the fine-grained region directly adjacent to the FZ due to grain boundary segregation and the subsequent pinning of the grains, since temperatures are lower in the other subzone, grain growth is not restricted in this way. The HAZ is a critical region in a weldment and is often the site of failure [20–22].

The fine-grained HAZ could also be referred to as a PMZ due to the incipient melting/liquation of the grain boundaries (Fig. 1.2).

1.2.2. Weld cracking in IN718

The severe thermal cycle and high restraint involved during the welding of high strength metals can cause cracks to develop. Some common types are:

Please cite this article as: S. Tamil Prabakaran, P. Sakthivel, M. Shanmugam et al., Modelling and experimental validation of TIG welding of INCONEL 718, Materials Today: Proceedings, https://doi.org/10.1016/j.matpr.2020.07.482

Table 2.1
IN718 chemical compositions.

Component	C	Cr	Fe	Mn	Ni	Nb	S	Si	Al	Ti	Co
Wt. %	0.03	18.12	19.07	0.07	53.24	5.0	0.001	0.11	0.52	0.94	0.09

Table 2.2
IN 718 mechanical and thermophysical data.

Density	8.22 g/cm^3
Melting Range	1336–1400 °C
Yield Strength Min (0.2% offset)	1,035 MPa
Ultimate Tensile Strength Min	1,240 MPa
Heat of dissolution of precipitate	100 J/g
Heat of fusion of matrix	320 J/g
Heat capacity: Matrix (Fe + Ni + Cr):	$0.439 + 14.62 \times 10^{-5}T–0.015 \times 10^{5}T^{-2}$ J/K g
Heat capacity: Nb Heat of fusion	$0.25 + 4.325 \times 10^{-5}T$ J/K g
Heat capacity: NbC	$0.43 + 6.95 \times 10^{-5}T–0.087 \times 10^{5}T^{-2}$ J/K g
Thermal conductivity: Matrix	$0.1145 + 0.0130156 \times T + 0.07772 \times 10^{-6}T^{2}$ W/cmK
Coefficient of thermal expansion	14.4×10^{-6} cm/cm K
Diffusion coefficient: Nb in matrix	$300 \times \exp(-35{,}800\,T)$ cm^2/s
Diffusion coefficient: Nb in liquid	10^{-5}cm^2/s

Table 2.3
Welding parameters.

S. No	Current	Velocity mm/s	Shield gas flow rate L/h	Observation
1	150	2.5	5	Center line hot crack
2	100	2.5	5	Center line hot crack
3	70	2.5	5	Center line hot crack
4	60	2.5	5	No Center line hot crack but under cut
5	50	2.5	5	No Center line hot crack, Full penetration
6	40	2.5	5	Lack of penetration

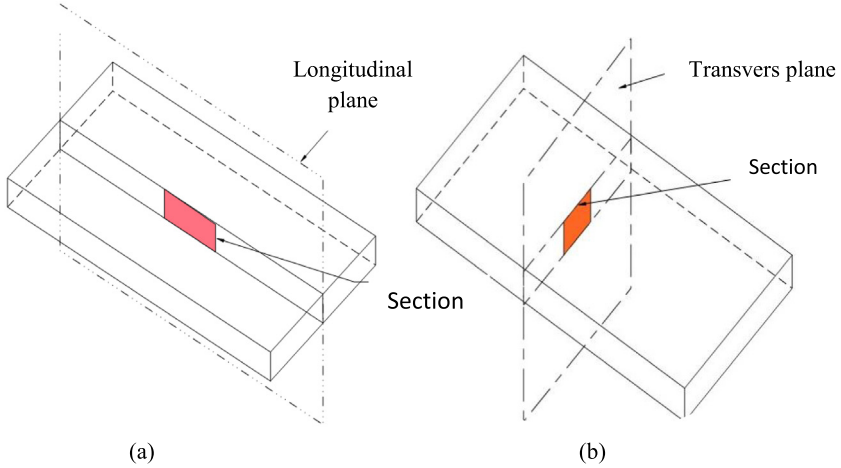

Fig. 2.4. Schematic diagram to specify the sample face a) Longitudinal plane b) Transvers plane.

Solidification or hot cracking: occurs in the weld as it solidifies due to the influence of tensile residual stress acting on low temperature melting phases that form as a result of segregation liquation cracking or microfissuring: occurs at grain boundaries in the HAZ due to segregation aggravated by the melting of the boundaries

1.3. Tungsten inert gas (TIG) welding

TIG welding is an electric arc welding process that uses a non-consumable tungsten electrode to produce the weld and an inert gas for shielding from atmospheric contamination (Fig. 1.3). ASM handbook defines a welding arc as 'a sustained electrical discharge through a high-temperature conducting plasma producing sufficient thermal energy so as to be useful for the joining of metals by fusion' [23–26].

Certain stable higher density metal (e.g. zirconium, thorium, lanthanum) oxides are often alloyed with tungsten to produce an electrode with superior properties to that of pure tungsten (minimum 99.5% by weight with no internal alloying elements). The oxides lower the work function of the electrode, which effectively

Please cite this article as: S. Tamil Prabakaran, P. Sakthivel, M. Shanmugam et al., Modelling and experimental validation of TIG welding of INCONEL 718, Materials Today: Proceedings, https://doi.org/10.1016/j.matpr.2020.07.482

Table 2.4
Values of semi axis.

Semi axis	Plane of measurement	Values in mm
B	Transverse plane	1.3
C	Longitudinal plane	1.192
A_f	Longitudinal plane	1.592
A_r	Longitudinal plane	2.52

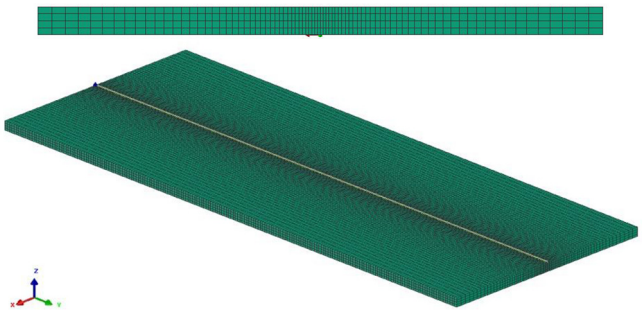

Fig. 2.5. Schmatic digram of weld plate.

means a reduction in the amount of energy required to give off an electron (i.e. to allow current to flow), lowering the voltage necessary to strike an arc (thus making it easier). Since the oxides are insulators and pure tungsten is a metallic conductor, oxide addition also increases the current carrying capability of the electrode [27,28]. The key advantage of TIG welding is that it allows for high precision, pure welds that are highly resistant to corrosion and cracking over long time periods. This makes TIG the welding procedure of choice for critical welding operations like sealing spent nuclear fuel canisters before burial. TIG welding creates no slag and no spatter since both are contained by the inert gas that shields the weld, making TIG welding a relatively clean and time efficient process. The concentrated nature of the TIG arc is one of its strong points. Welds of great strength and quality can be made with thin materials, light materials, dissimilar materials, in most available metals, and all with minimal distortion or corruption of the adjoining base metal. However, TIG welding does have disadvantages [29,30]. Therefore, it is clear that precise selection of the process parameters is necessary.

The principle operating variables for GTAW are:

- arc voltage (arc length),
- welding current,
- welding speed (and filler wire feed rate if applicable), and
- shielding gas (inert gas such as argon or helium)

All of these variables interact with each other very strongly; therefore, they cannot be treated as independent variables while establishing welding procedures for fabricating specific joints.

2. Methodology

The development of numerical model involved modeling of moving heat source and simulation with experimental welding parameters and experimental validation. Sequences of the work or methodology of project work has been explained in the flow chart Fig. 2.1.

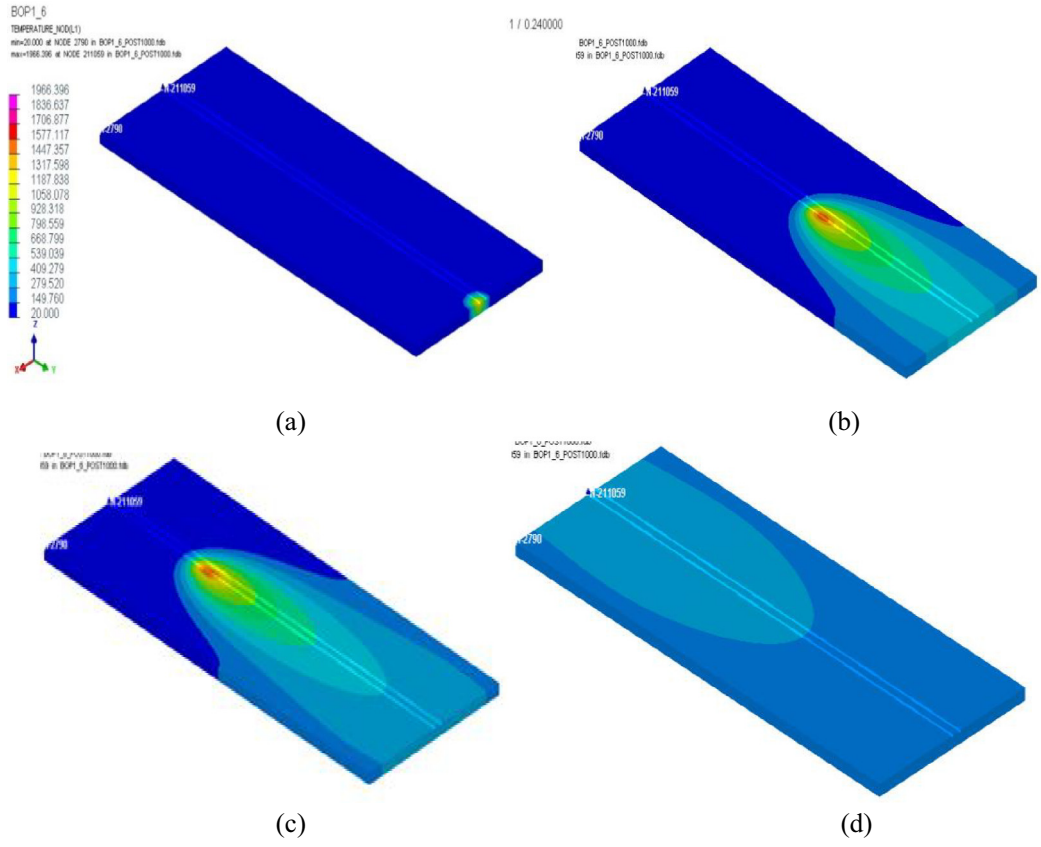

Fig. 2.8. Temperature distribution at different instent time on top suface (a) time at 0 s (b) time at 20 s (c) time at 30 s (d) time at 800 s.

Please cite this article as: S. Tamil Prabakaran, P. Sakthivel, M. Shanmugam et al., Modelling and experimental validation of TIG welding of INCONEL 718, Materials Today: Proceedings, https://doi.org/10.1016/j.matpr.2020.07.482

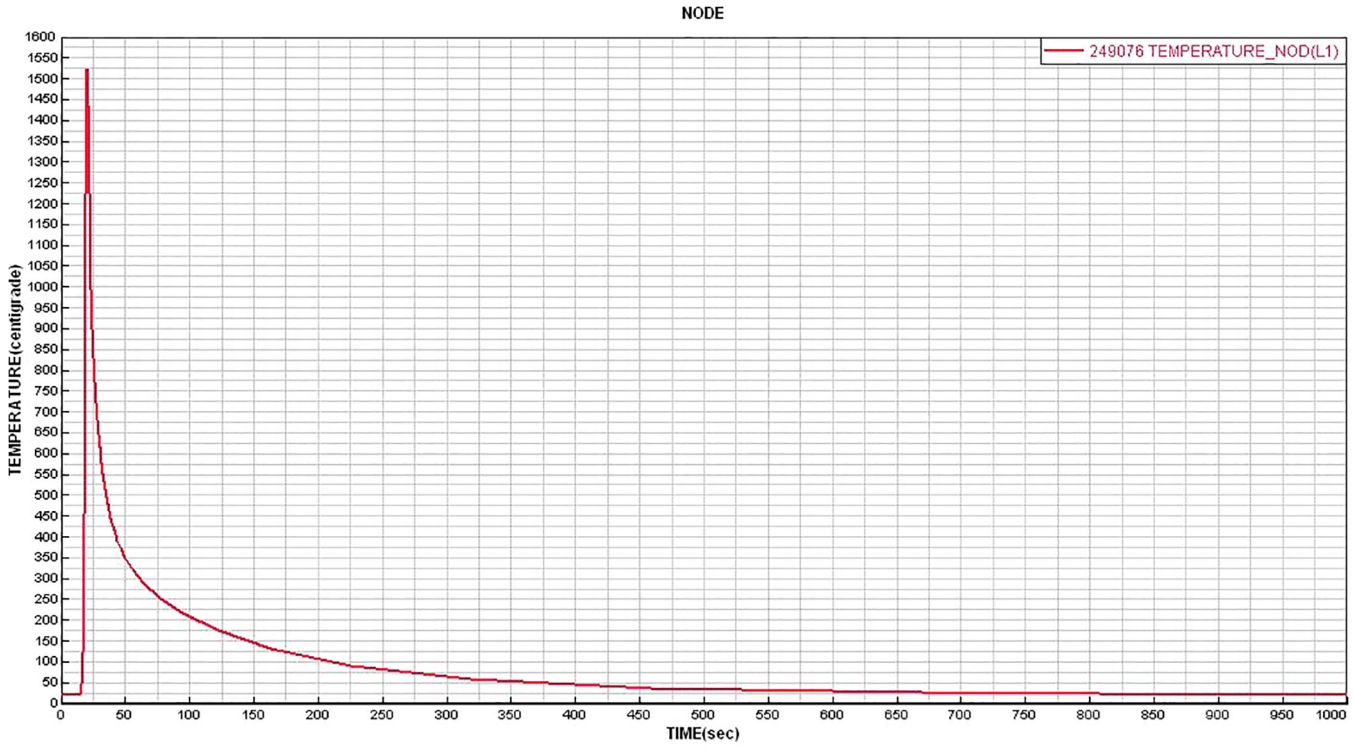

Fig. 2.9. Temperature history for the top surface of the weld centerline.

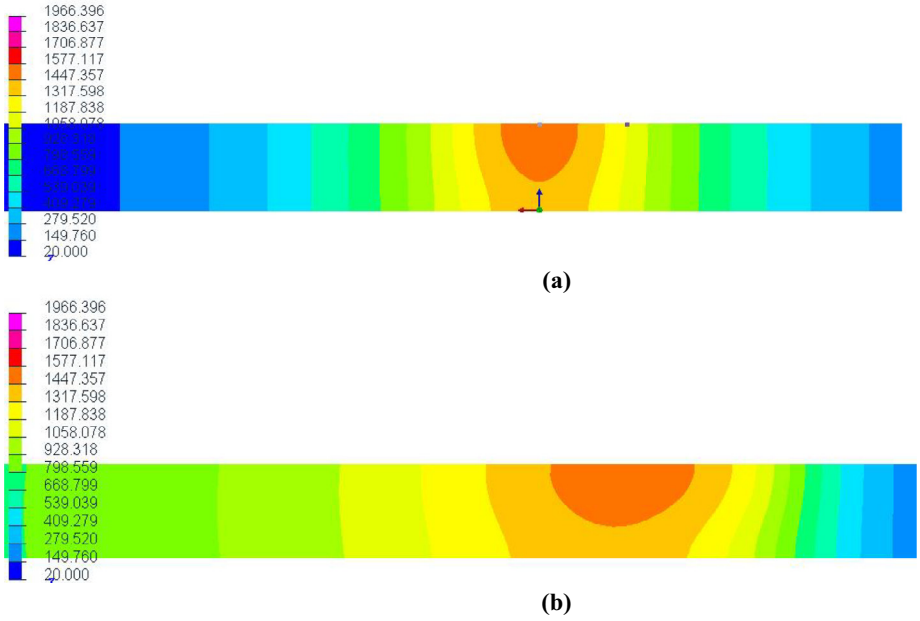

Fig. 2.10. Temperatures distribution in a cross section to the weld (a) Transverse section: (b) Longitudinal section:

Thermal and metallurgical aspects of TIG welding process have been studied for modelling input variables followed by simulation or solving and experimentally thermal history and fusion zone dimensions have been measured DAQ system for validating the model. Finally investigation of weldment has been done using simulation results.

2.1. Modeling

2.1.1. Model definition

Three dimensional (3D) IN718 plate welding analyses performed by Sequentially-coupled nonlinear thermal and elastic–plastic FE analyses are used to generate a welding simulation

Please cite this article as: S. Tamil Prabakaran, P. Sakthivel, M. Shanmugam et al., Modelling and experimental validation of TIG welding of INCONEL 718, Materials Today: Proceedings, https://doi.org/10.1016/j.matpr.2020.07.482

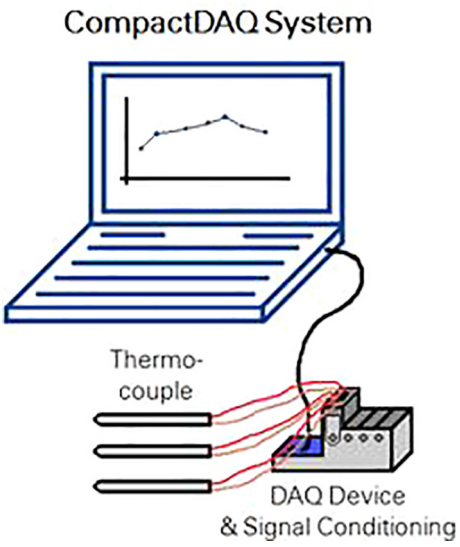

Fig. 3.1. Schematic diagram of DAQ setup.

model, capable of measuring thermal cycles and calculating the evolution of stress and deformation, and predicting the residual stresses and distortions that occur as a result of the welding process. The coupling procedure is illustrated in Fig. 2.2.

First, a conduction-based thermal analysis is run to determine the entire temperature history for each node in the FE mesh. This data is then used as input for a mechanical (stress-displacement) elastic–plastic analysis, which allows the thermal history and its mechanical effects to be equated via thermal expansion, hence changing thermal effects into mechanical behaviour. Any microstructural changes can also be determined using the temperature history and implemented in the mechanical analysis (Fig. 2.3).

3-Dimensional numerical simulations of fluid flow and heat transfer in transient TIG weld of IN718 using SYSWELG package.

2.1.2. Material properties

Chemical compositions of IN 718 are shown in Table 2.1 and thermophysical properties shown in Table 2.2 the empirical relationship for the variation of thermal conductivity of alloy IN 718 was taken from the work.

2.1.2.1. Bead on plate weld. Experimental study of TIG welding on 2 mm IN718 plate has been done with bead on plate welds for dif-

Fig. 3.2. Experimental setup.

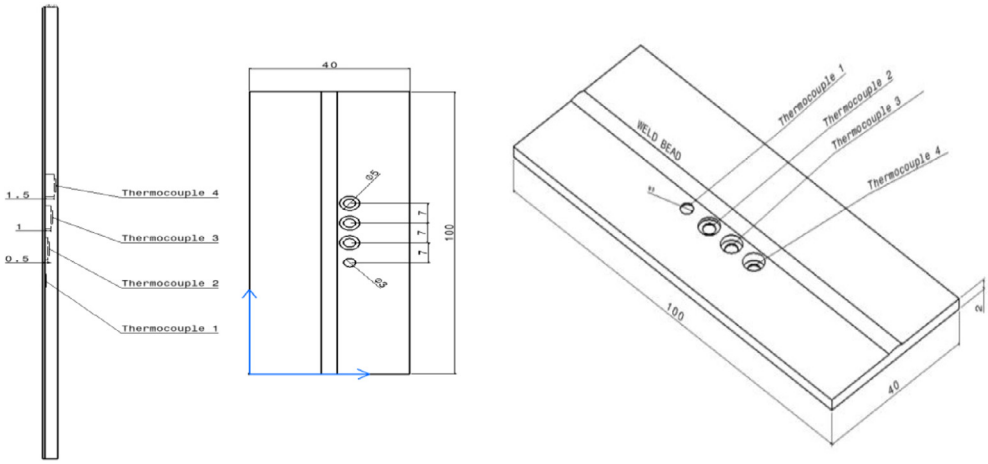

Fig. 3.3. Schematic diagram of weld plate and possession of thermocouple.

Please cite this article as: S. Tamil Prabakaran, P. Sakthivel, M. Shanmugam et al., Modelling and experimental validation of TIG welding of INCONEL 718, Materials Today: Proceedings, https://doi.org/10.1016/j.matpr.2020.07.482

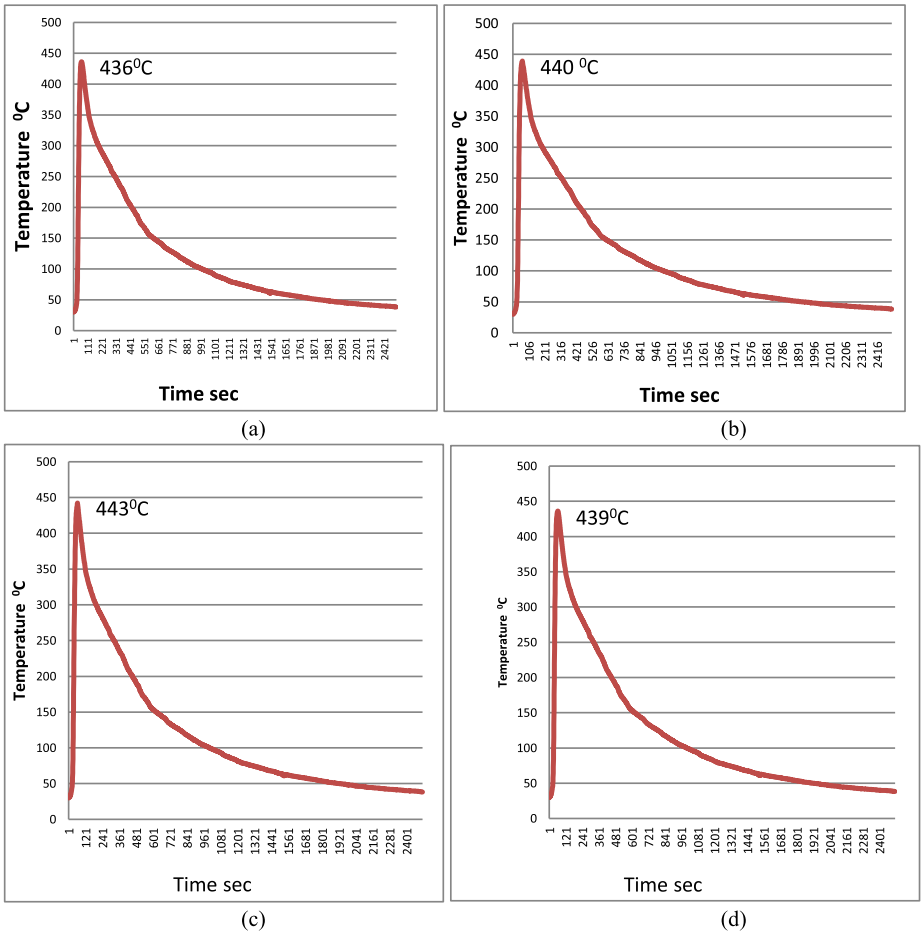

Fig. 3.4. Thermal cycle plots measured at four different planes from centre line of weld (a) top surface (b) 0.5 mm from top surface (c) 1 mm from top surface (d) 1.5 mm top surface.

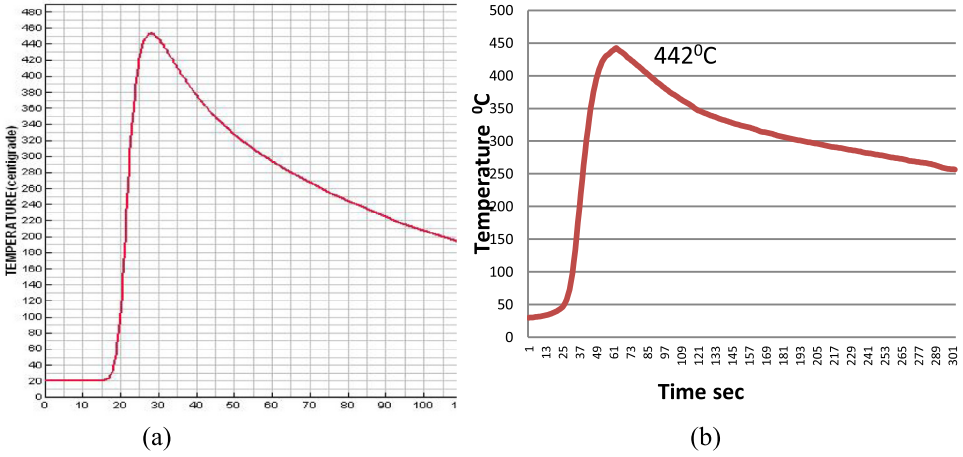

Fig. 4.1. Comparison of Thermal cycles measured from (a) FE model (b) experimental work.

ferent welding parameters Table 2.3. Except current all other welding parameters kept constant. Welding electrode diameter was 2.4 mm, DCEN welding polarity, stinger welding technique, manual and autogenously TIG welding.

2.1.2.2. Measuring semi axis. For defining the double ellipsoidal moving heat source required A_f, A_r, B, C semi axis which are estimated from cross sectional metallographic data and from weld pool surface ripple markings.

Direction of solidification always in the direction of maximum thermal gradient, orientation of columnar dendrite was perpendicular to the fusion line or liquids temperature isotherm (1336 °C). Fig. 2.4 have been used for measuring weld pool size and dates tabulated in Table 2.4.

Please cite this article as: S. Tamil Prabakaran, P. Sakthivel, M. Shanmugam et al., Modelling and experimental validation of TIG welding of INCONEL 718, Materials Today: Proceedings, https://doi.org/10.1016/j.matpr.2020.07.482

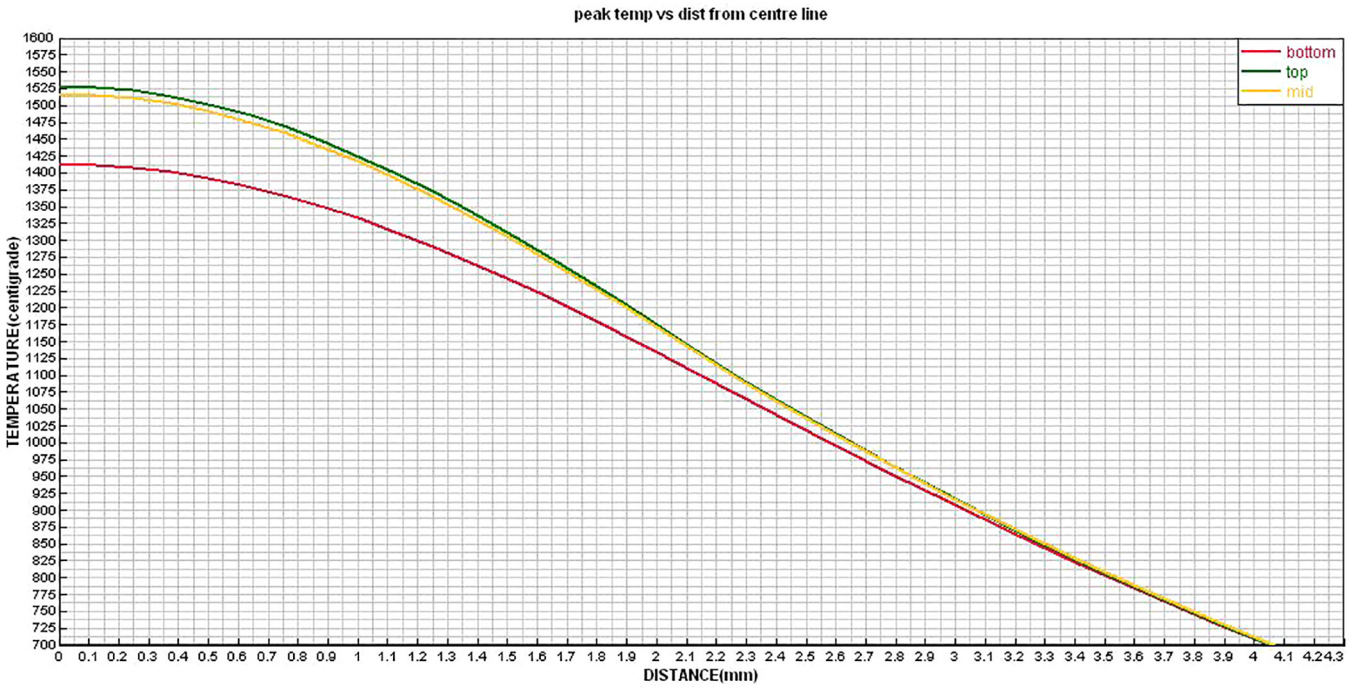

Fig. 4.2. temperature distance curve from weld centre line on top surface and plane 2 mm from top surface at time 20th sec.

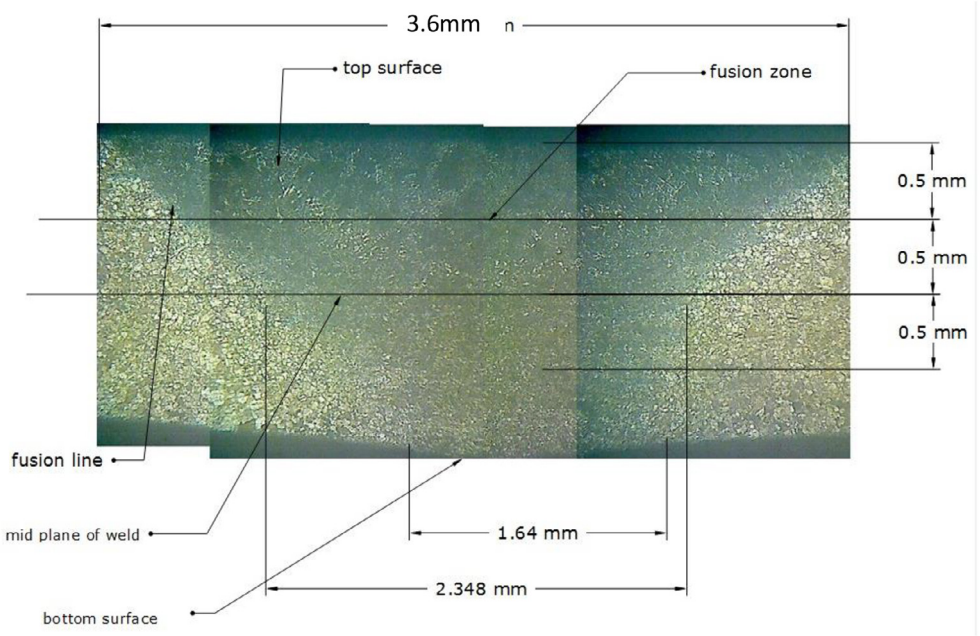

Fig. 4.3. Microstructure of weldment on transverse plane (200X).

Semi axis values where used as input of model SYSWELD heat source modeling for 2 mm IN718 plate.

2.2. Plate modeling

Weld plate modeled as 100 mm length with 100 divisions, 40 mm width with 80 divisions and thickness 2 mm with 4 divisions. Element size is made finer in weld zone since temperature gradient is high and coarser elements are used away from the weld zone, shown in Fig. 2.5.

2.3. Clamping condition

Weld plate is rigidly fixed at corners by constrained the nodes at corners have zero displacement. This clamping condition defines the boundary condition to the mechanical analysis.

2.4. Simulation

As double ellipsoidal heat source used for simulate the TIG welding of IN718, from Table 2.1. Welding parameters traverse

Please cite this article as: S. Tamil Prabakaran, P. Sakthivel, M. Shanmugam et al., Modelling and experimental validation of TIG welding of INCONEL 718, Materials Today: Proceedings, https://doi.org/10.1016/j.matpr.2020.07.482

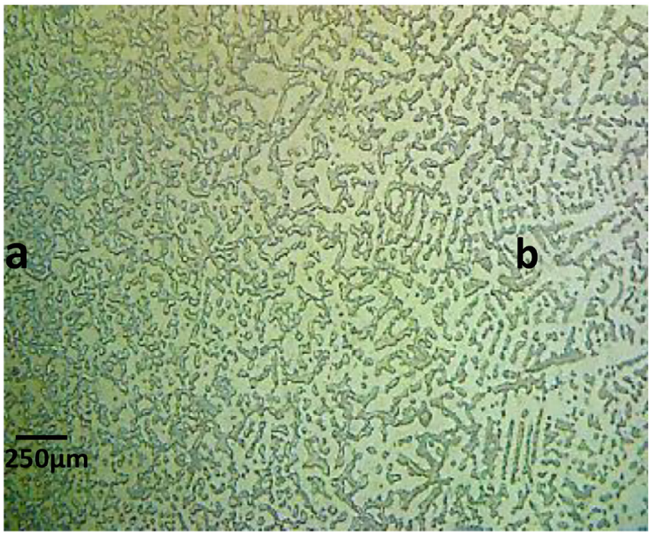

Fig. 4.5. Microstructures 200X (a) centre line of weld fine equaxid grains (b) Away from centre line coarse grains.

speed 2.5 mm, current 50 A, voltage 22 V and arc efficiency 57% has been taken from previous research work, from equation *Q* is the energy or power input is 440 W along with non linear thermo physical properties (Table 2.2) have been used while solving the model in transient condition.

Fig 2.9. shows the temperature history for a point on the top surface at the weld centerline of FE weld model, the maximum temperature 1525 °C is achieved at 20 s and cooling is complete after approximately 800 s. The temperature distribution approximately midway through the welding process is shown in Fig. 2.8.

Fig. 2.8 shows the isotherms of different temperature that is interface of two different colors, each color indicating respective constant temperature. Fusion temperature of IN718 is 1336 °C, isotherm 1336 °C indicating fusion line, zone within isotherm (>1336 °C) indicating fusion zone. Prediction of fusion zone, HAZ, PMZ size and shape of them are possible (Fig 2.10).

3. Experimental work

3.1. Measuring thermal history

Measuring thermalcycles have been done by using thermocouple and NI-DAQ setup at the time weld the sample, online thermalcycle measuring setup shown in schematic diagram Fig. 3.1 weld sample (100 mm long 40 mm width and 2 mm thick IN718 plate) was prepared and clamped on work table as shown Fig. 3.1.

There were four K-type thermocouple (chromal-alumel) attached to the sample 6 mm from centre line of the weld with 7 mm pitch as shown in Fig. 3.2 in thickness array with 0.5 mm gap between successive thermocouples. DAQ signals were decoded in signal express 2011 package as temperature–time plot (Fig. 3.3).

Peak temperature on top plane, plane at 0.5 mm, 1 mm and 1.5 mm from top surface read respectively 436 °C, 440 °C, 443 °C and 439 °C. Location of probe 6 mm away from centre line of the weld, middle portion of the material in than bottom and top surface due to convective heat loss and there is no contacted with heat source. Except peak temperature slope of the plot (heating and cooling rate) (Fig. 3.4).

3.1.1. Metallographic technique

Metallographic samples of weld of alloy IN718 were prepared for metallographic examination by first grinding through 600A paper, polishing through to ¼ μ diamond paste and then final polishing with slurry. Electrolytic etching was carried out using following etchant: 1part chromic acid (5%) + 1 part sulphuric acid methanol (10%).

4. Validation and discussion

It comprises validation of q model and investigation of weldment. Model validated with two different aspects, comparing thermal cycles and fusion zone dimensions.

4.1. Validation of the FE model

The validation of model includes Comparison of thermal cycles which are measured by experimental work and numerical modelling and size of the fusion zone measured by experimental work and numerical model result.

4.1.1. Comparison of thermal cycles

Based on the Experiment and FE analysis, the thermal heat source profiles were obtained as shown in Fig. 4.1.

Experimental peak temperature 442 °C from Fig. 4.1(b) and FE model peak temperature 453 °C from Fig. 4.1 and it describes the comparison of the peak temperatures of experimental and FEM of location at 50 mm from starting point of weld and 6 mm from centre line of the weld in transverse direction on plane which 1 mm from top surface, measured peak temperature of FE model is 453 °C and peak temperature of experimental 442 °C. Variation of FEM peak temperature is 2%.

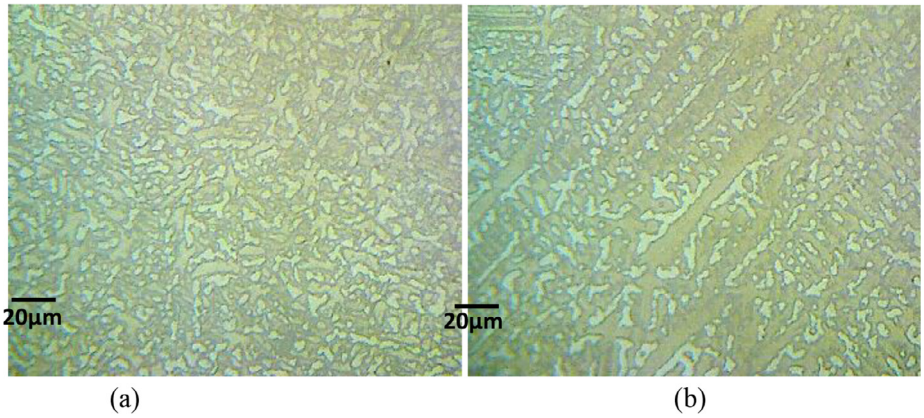

Fig. 4.6. Microstructures 500X at (a) centre line of weld fine equaxid grains (b) Near to fusion line.

Please cite this article as: S. Tamil Prabakaran, P. Sakthivel, M. Shanmugam et al., Modelling and experimental validation of TIG welding of INCONEL 718, Materials Today: Proceedings, https://doi.org/10.1016/j.matpr.2020.07.482

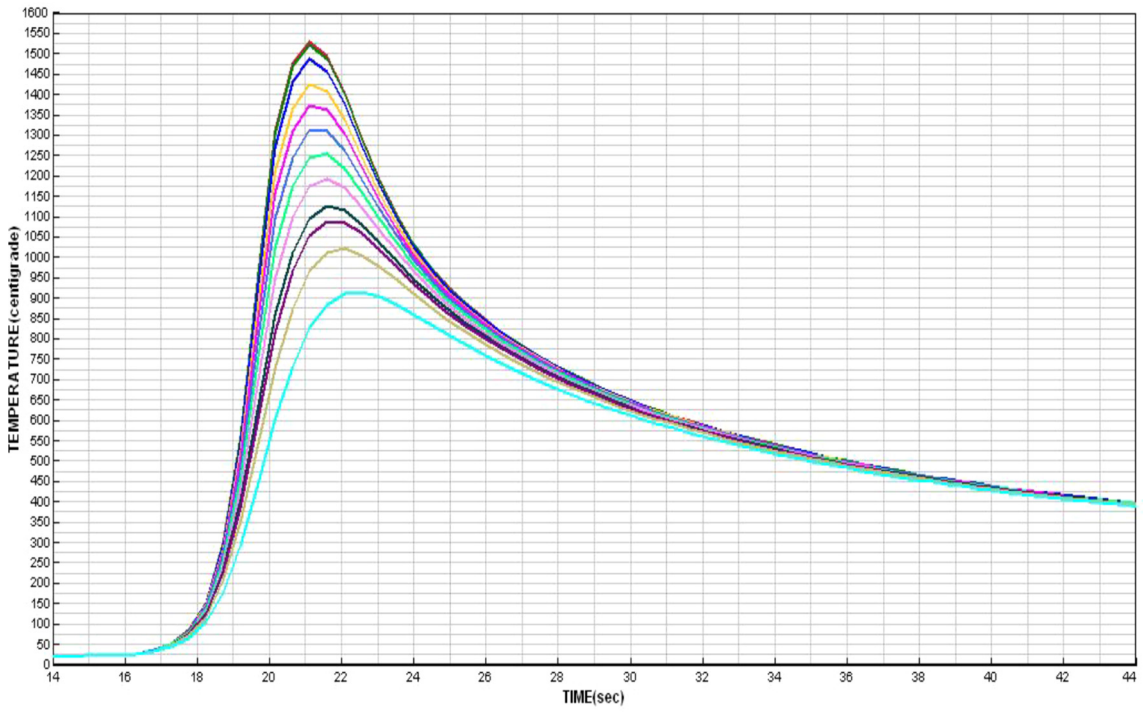

Fig. 4.7. Thermal cycle from centre line of weld to one edge of plate on top plane.

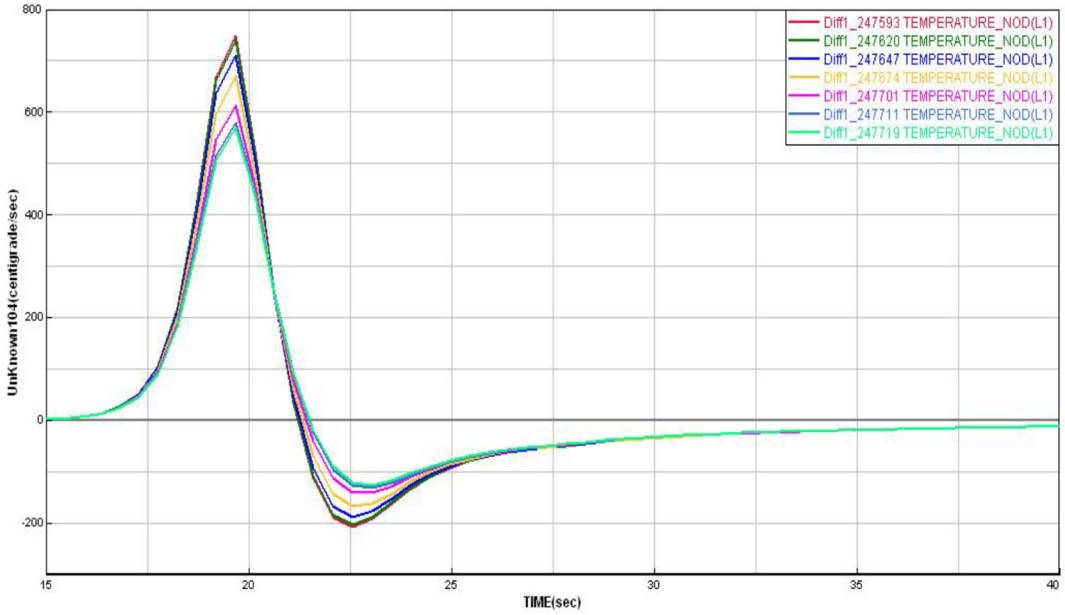

Fig. 4.8. Cooling rate curves from centre line of weld to one edge of plate on top surface.

4.1.2. Fusion zone size and shape comparison

Based on the FE analysis, the width of bead on three different planes was obtained from temperature distance plot as shown in Fig. 4.2 and dimensions were list at quasi steady state condition.

Based on the metallurgical technique, the width of bead on three different planes was obtained from microstructure of transverse cross section fusion zone shown in Fig. 4.3.

The half width of the fusion zone (FZ) (temperature >1336 °C the melting point of IN718) here is ≈1.4 mm for the top surface, 1.35 mm for middle plane and ≈0.95 mm for the bottom surface (see Fig. 4.2), which compares well with measurements of half an actual weld (top surface ≈1.59 mm, middle plane≈1.17 mm and bottom surface ≈0.82 mm (Figs. 4.4–4.7).

4.2. Investigation of IN718 weldment

4.2.1. Effect of peak temperature and cooling rate

Corresponding to composition of alloy 718 (Nb 5%) the pseudo binary phase diagram is shown in Fig. 4.8 reveals the important thermo physical properties, for example liquids temperature 1400 °C, solids temperature 1336 °C, eutectic temperature 1175 °C which are helped to measure the dimensions of FZ, HAZ.

Please cite this article as: S. Tamil Prabakaran, P. Sakthivel, M. Shanmugam et al., Modelling and experimental validation of TIG welding of INCONEL 718, Materials Today: Proceedings, https://doi.org/10.1016/j.matpr.2020.07.482

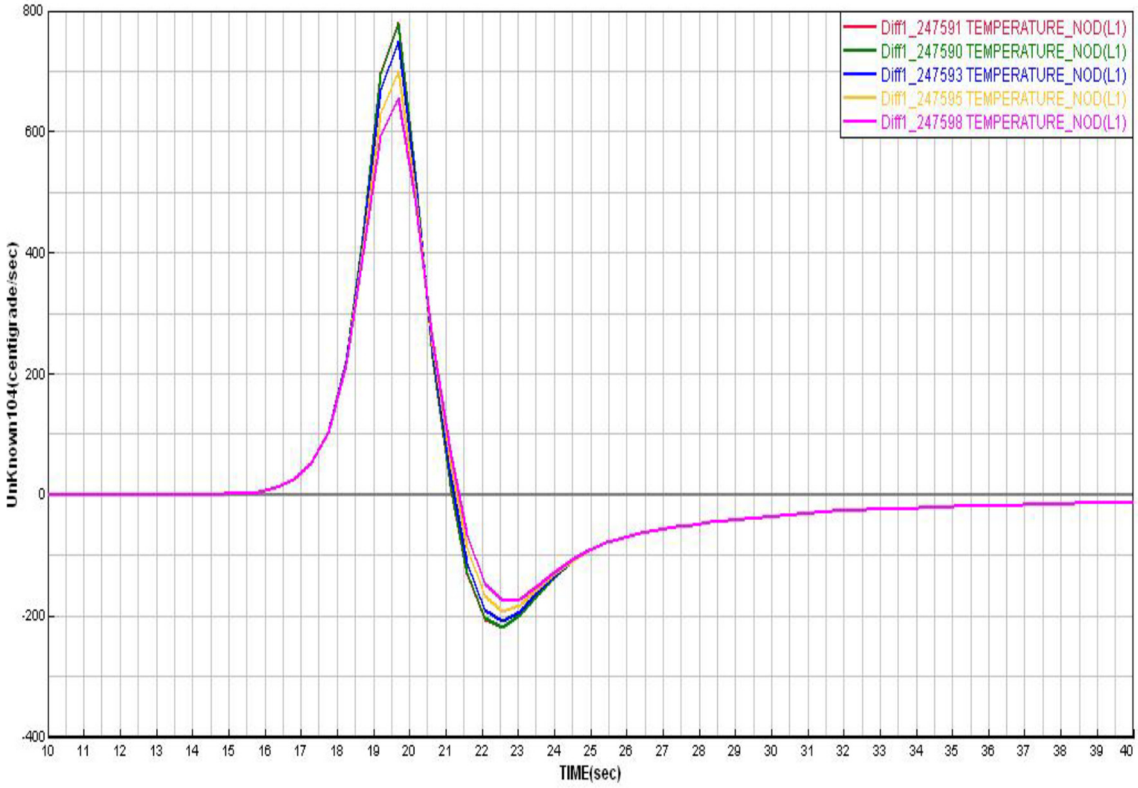

Fig. 4.9. Cooling rate curves from centre line of weld to one edge of plate on middle plane.

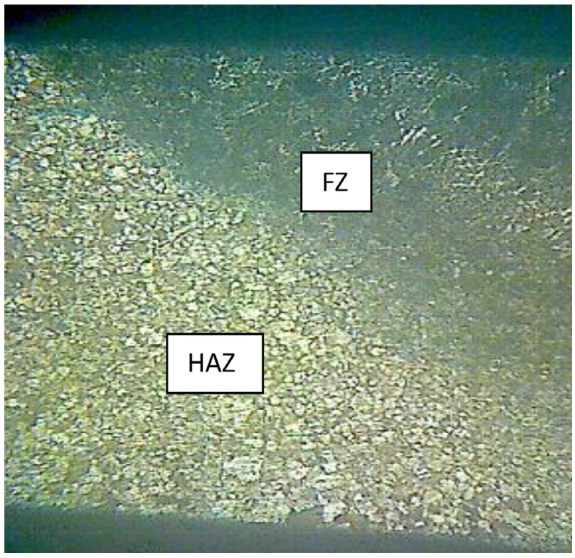

Fig. 4.10. Microstructures 200X coarse grains at HAZ.

It has been observed that the higher the cooling rate, that is, shorter the solidification time, the finer the dendritic structure in the fusion zone. Dendrite arm spacing is function of the cooling rate or solidification time. Slower the cooling rates during solidification, the longer the time available for coarsening and longer the dendrite arm spacing.

Fig. 4.8 shows cooling rate curves on top plane, higher the cooling rate about 200 °C/sec at centre line of weld and lowering away from centre line of weld hence finer grains at centre line and coarser near to fusion line in the top plane of weld.

Fig. 4.9 shows the cooling rate curves on the transverse plane, high cooling rate observed at middle plane compare to top and bottom plane of plate it reveals that grains are finer at middle plane compare to top and bottom plane.

Whenever the material experiences the peak temperature above recrystallization temperature and below melting point temperature gain growth taking place, zone known as HAZ Fig. 4.10.

Dimensions of Fusion zone FZ width and heat affected zone HAZ on three different planes have been measured with the help of isotherms and temperature vs distance curve from Fig. 4.11. Width of the fusion zone measured by liquids temperature isotherm and width of the HAZ is measured distance between eutectic temperature and liquids temperature which are listed out in Table 4.5.

4.2.2. Susceptibility of HAZ hot cracking

The objective of this discussion is investigation of the formation and solidification of the grain boundary liquid in the subsolidus HAZ and type of stress distribution with help of thermo cycles obtained of numerical model.

Zone where peak temperature observed between solids temperature 1400 °C and eutectic temperature 1175 °C is known HAZ and temperature range from 1225 °C to solids temperature 1327 ^{0}C corresponds to the remaining portion of the thermal cycle during which the precipitate is fully liquated and metastable liquid produced by precipitate liquation coexists with the matrix (Fig. 4.12).

4.2.2.1. HAZ hot crack susceptibility. Variables affecting Hot Cracking Susceptibility on HAZ depends on many factors for example peak temperature, Heating and cooling rates, Initial precipitate film thickness, and tensile residual stress etc. within HAZ only particular distance have higher hot crock susceptibility depends on above factors.

Please cite this article as: S. Tamil Prabakaran, P. Sakthivel, M. Shanmugam et al., Modelling and experimental validation of TIG welding of INCONEL 718, Materials Today: Proceedings, https://doi.org/10.1016/j.matpr.2020.07.482

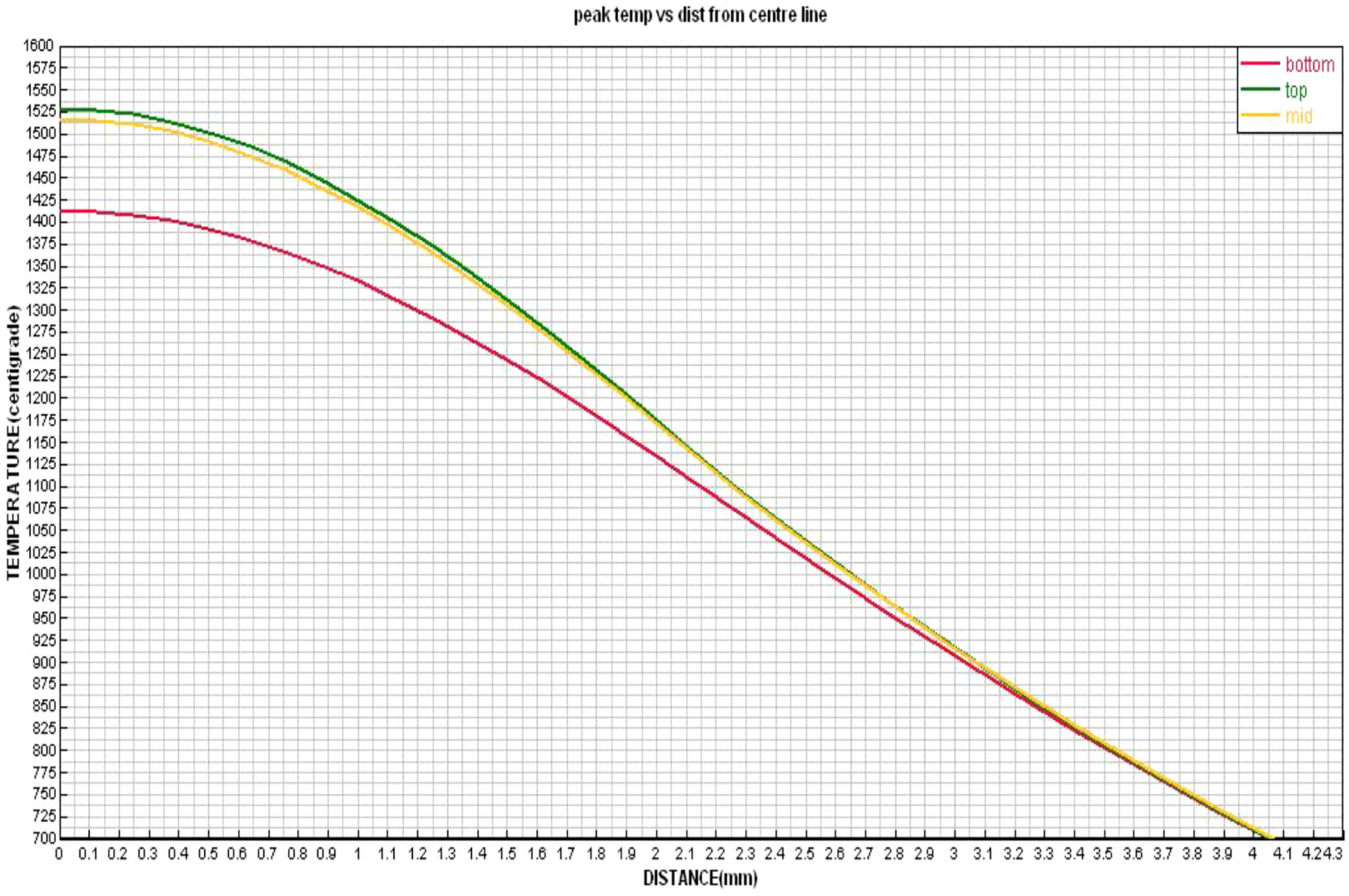

Fig. 4.11. Temperature distance curve from centre line of weld to one edge of plate.

Table 4.5
Dimensions of weldment.

	Top plane	Middle plane	Bottom plane
Width of FZ half width	1.4 mm	1.35 mm	0.0.95 mm
Width of HAZ	0.63 mm	0.66 mm	0.85 mm

Grain boundary films form in the subsolidus HAZ as a consequence of constitutional liquation. Liquation cracking in the subsolidus portion of the HAZ is due to the formation of grain boundary liquid through constitutional liquation of precipitates and the inability of the liquid films to support tensile stresses which develop during cooling of the weld HAZ. In general, the transient stress in the HAZ becomes tensile only after the HAZ has cooled through a certain temperature below the peak temperature. At any given HAZ location, the time at which the stress becomes tensile depends upon several factors, such as the specific heat input, the thermophysical properties of the alloy, and the alloy's high temperature mechanical behavior.

Since liquation cracking depends on the simultaneous existence of the liquid film and tensile stress, it becomes important to be able to predict the rate of formation and solidification of grain boundary films under various welding conditions. Liquation cracking susceptibility in the subsolidus HAZ can be predicted by appropriately combining models of transient stress generation with a model for microstructural evolution which deals with the formation and solidification of grain boundary liquid (Fig. 4.13).

In further discussion susceptibility of hot crack in INCONEL 718 weldment investigated in the temperature range from 1225 °C to solids temperature 1327 °C only because which have more impact on variables affecting Hot Crack susceptibility on HAZ as follows.

4.2.2.2. Heating and cooling rate. The thickness of the residual grain boundary liquid film at a given HAZ location during temperature range from 1225 °C to solids temperature 1327 °C depends on the heating and cooling rates. It can be seen from Fig. 4.14 that the film thickness decreases with decreasing heating and cooling rates and vanishes completely for processes employing heating and cooling rates less than about 17 K/s and maximum at intermediate cooling rates (100 and 1000 K/s), the net interface velocity depends upon the relative contributions of the two competing velocity components: the solidification component due to back diffusion and the melting component due to the concentration gradient across the liquid film.

If the transient stress in the HAZ location is in tensile at the eutectic temperature on cooling, amount of stress depends on cooling rate, it can be concluded that low heating and cooling rates are less likely to produce liquation cracking than higher heating and cooling rates. However, the transient stress pattern in the HAZ also depends on the heating and cooling rates employed. Figs. 4.15 and 4.16 shows tensile stress distributed in fusion and HAZ about 650 N/m^2 of FE model.

4.2.2.3. Peak temperature. Fig. 4.15. Shows peak temperature increase as the fusion zone is approached, the heating rate also increased correspondingly, the heating rate is 575 °C/s at 1225 °C isotherm, the heating rate at 1327 °C isotherm is 625 °C/s cooling rate is 125 °C/sec at 1327 °C and 150 °C/sec at 1227 °C. which are within the range of 100 °C/s and 1000 °C/s Although the difference

Please cite this article as: S. Tamil Prabakaran, P. Sakthivel, M. Shanmugam et al., Modelling and experimental validation of TIG welding of INCONEL 718, Materials Today: Proceedings, https://doi.org/10.1016/j.matpr.2020.07.482

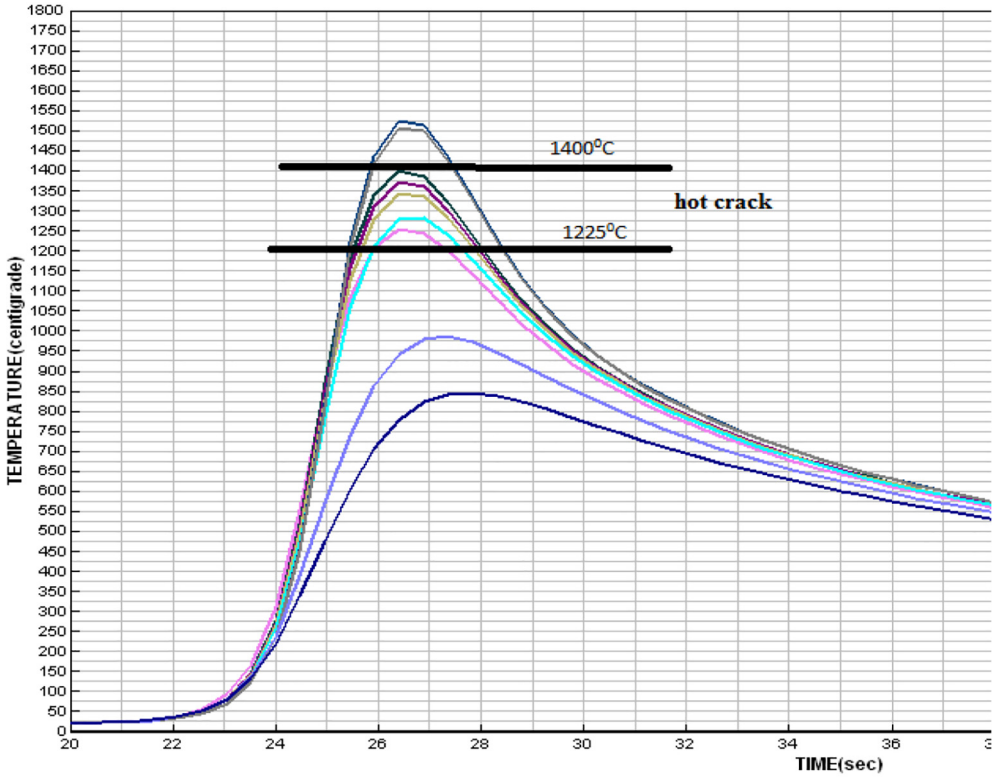

Fig. 4.12. Thermal cycles at transverse direction from centre line of weld on top plane.

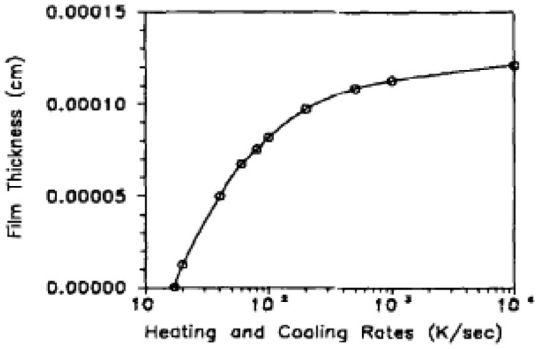

Fig. 4.13. Film thickness as a faction of heating and cooling rates [6].

in the heating/cooling rates between the two locations is not very significant, the residual film thickness at the eutectic temperature is significantly lower at the 1327 °C isotherm than at the 1225 °C isotherm, This is because of the additional time available for solute back diffusion in the matrix during heating and cooling in the 1225 °C to 1327 °C temperature range. Hence, the HAZ microstructure at room temperature will consist of a greater volume fraction of the second phase at the 1225 °C isotherm location than the 1327 °C isotherm location. However, this does not lead to the conclusion that the 1225 °C isotherm location is more susceptible to cracking than the locations closer to the fusion zone. This is because the residual film thickness at any time during cooling is higher at locations closer to the fusion zone. Notice that the residual film thickness at the 1327 °C isotherm location is higher than that at the 1225 °C isotherm location at any time during peak temperature range (1400–1175 °C). Also, the 1327 °C isotherm location will continue to have a grain boundary film even after the film at the 1225 °C isotherm location has completely solidified. Hence locations closer to the fusion zone are still preferred sites for crack nucleation (Fig 4.18).

Susceptibility of hot crack on INCONEL 718 HAZ is in between the temperature range of 1225–1327 °C especially near to the fusion line that is near to the temperature 1327 °C isotherm. With help of above details we can predict that the location of hot crack susceptible zone 1.375 mm from centre line of the weld and width 0.375 mm.

5. Conclusions

The peak temperatures on middle surface at 6 mm from centre line of weld were observed using experimental work (442 °C) and FE model (453 °C) which ensures that the process has negligible temperature change at the quasi-steady state condition. There is good agreement between the predicted and measured thermal cycles.

The fusion zone shapes and size were observed by the experiment and by numerical model are found to be in good agreement in quasi-steady state condition. The half width of the FZ is 1.4 mm for the top surface, 1.35 mm for middle plane and 0.95 mm for the bottom surface, which compares well with measurements of half an actual weld on top surface 1.59 mm, middle plane 1.17 mm and bottom surface 0.82 mm.

Predicted half width of FZ and HAZ respectively on top surface 1.4 mm and 0.63 mm, middle plane 1.35 mm and 0.66 mm and bottom surface 0.95 mm and 0.85 mm.

Susceptibility of hot crack on INCONEL 718 HAZ is in between the temperature range of 1225–1327 °C especially near to the fusion line that is near to the temperature 1327 °C isotherm. Predicted susceptible location of hot crack zone is 1.375 mm from centre line of the weld and width 0.375 mm.

Please cite this article as: S. Tamil Prabakaran, P. Sakthivel, M. Shanmugam et al., Modelling and experimental validation of TIG welding of INCONEL 718, Materials Today: Proceedings, https://doi.org/10.1016/j.matpr.2020.07.482

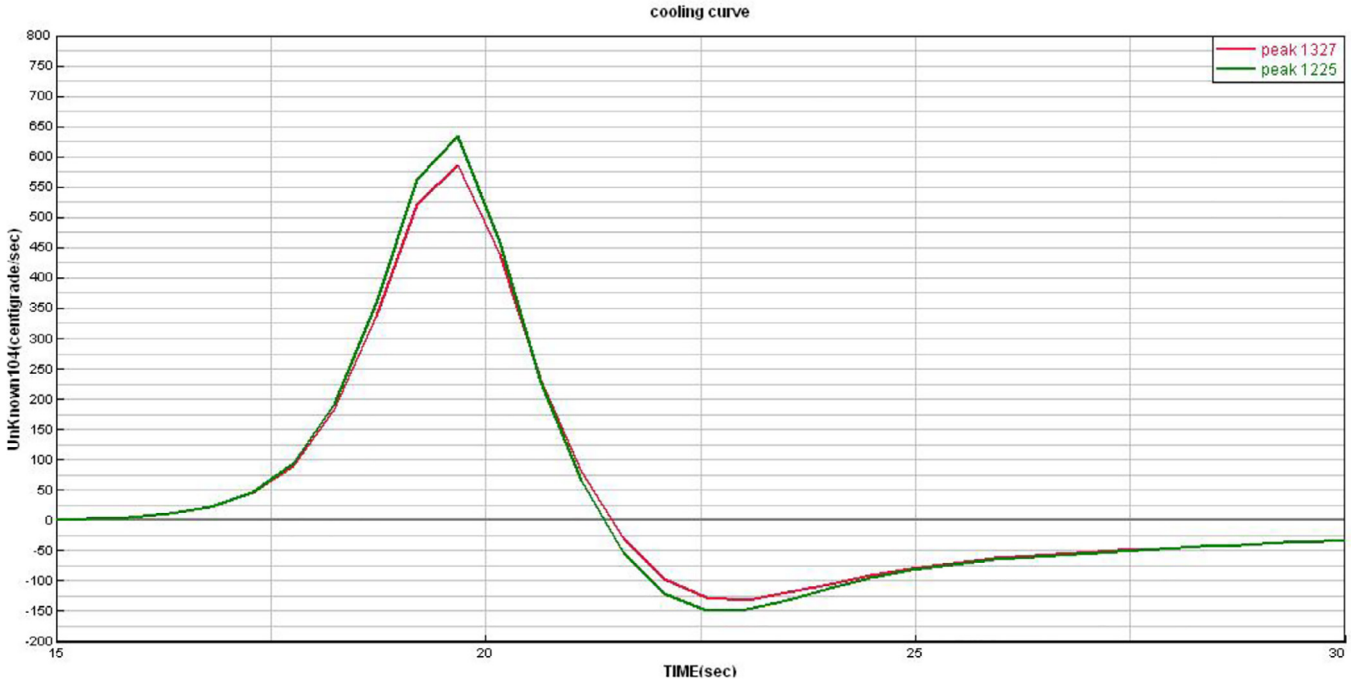

Fig. 4.14. Cooling rates at (1) peak temperature 1327 °C (2) peak temperature 1225 °C.

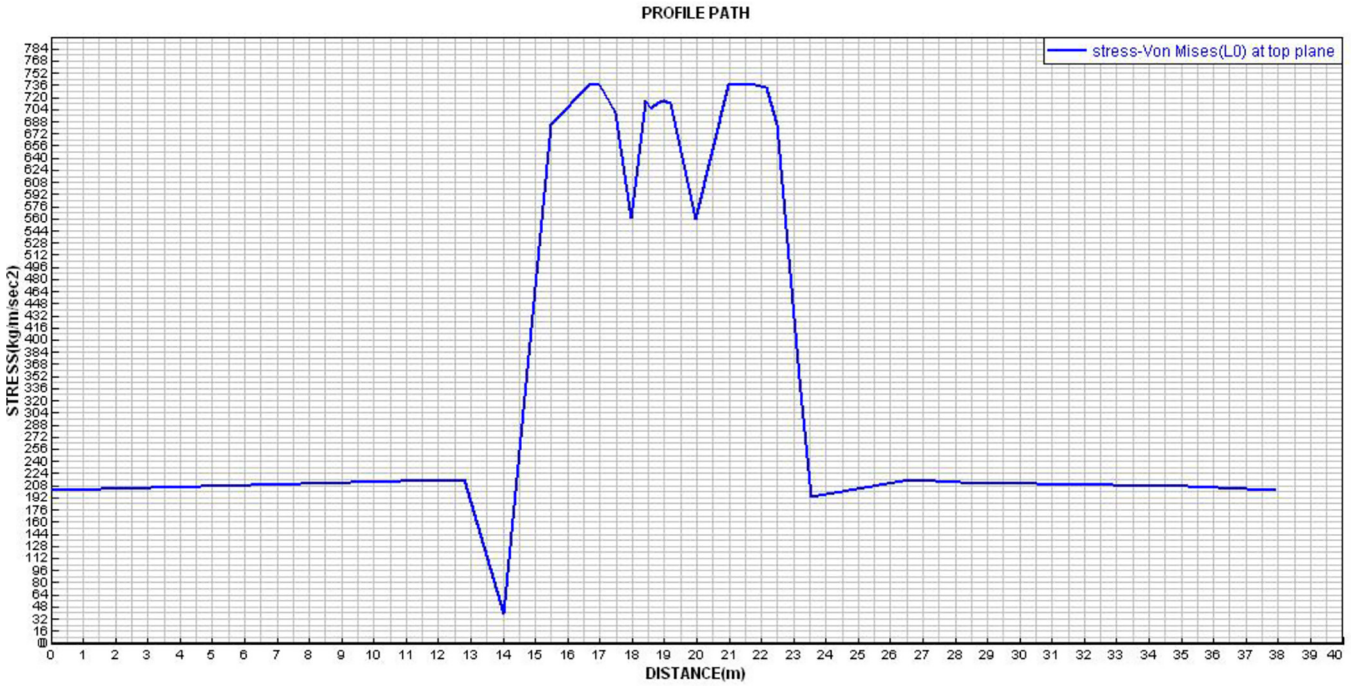

Fig. 4.15. Stress distribution along transverse direction on top plane at instant time 20th sec and middle of the weld.

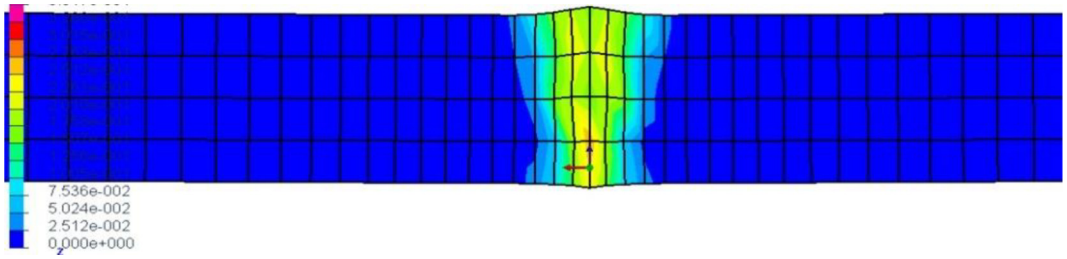

Fig. 4.16. Stress distribution along transverse direction on top plane at instant time 20th s and middle of the weld.

Please cite this article as: S. Tamil Prabakaran, P. Sakthivel, M. Shanmugam et al., Modelling and experimental validation of TIG welding of INCONEL 718, Materials Today: Proceedings, https://doi.org/10.1016/j.matpr.2020.07.482

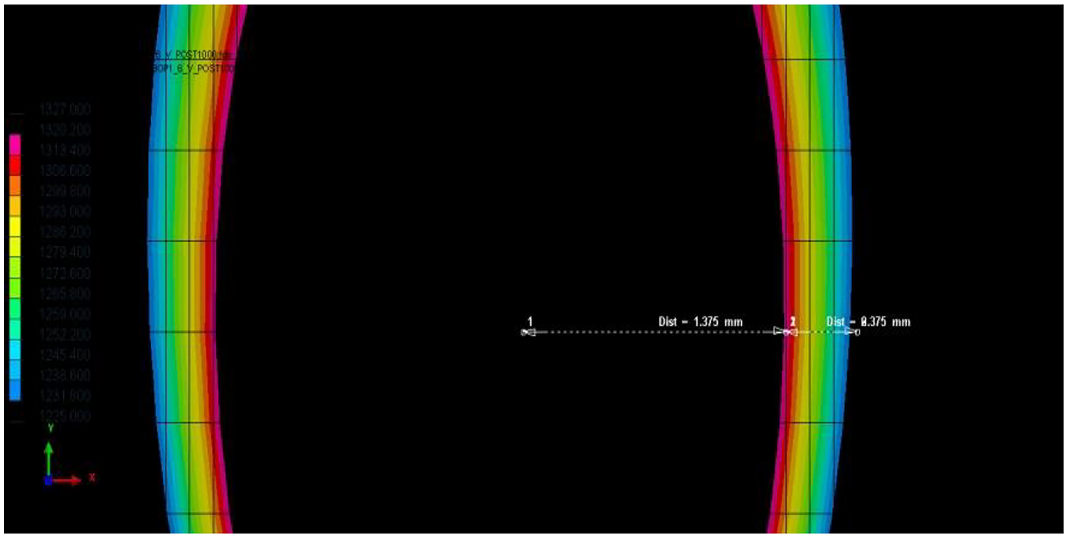

Fig. 4.17. HAZ hot crack susceptibility zone.

Declaration of Competing Interest

The authors declare that they have no known competing financial interests or personal relationships that could have appeared to influence the work reported in this paper.

References

[1] Y. Song, A.A. Becker, T.H. Hyde, P. Andrews, P. Spiller, Mechanical Properties of INCO718 Superalloy at High Temperatures, in: Proceedings of the International Conference on Metal Fabrication and Welding Technology (METFAB), A.A. Becker (ed.), Nottingham, UK, pp. 233-244, 2003.

[2] D. Dye, Mechanical Effects Arising From the Welding Of Superalloys PhD Thesis, University of Cambridge, UK, 2000, p. 154.

[3] H.D. Hibbitt, P.V. Marcal, A. Numerical, Thermo-mechanical model for the welding and subsequent loading of a fabricated structure, Comput. Struct. 3 (1973) 1145–1174.

[4] Welding Handbook, vol. 2: Welding Processes, 8th ed. Miami, FL, USA: American Welding Society (AWS), 1991.

[5] K. Masubuchi, Analysis of welded structures: residual stresses, distortion and their consequences 1ed, Pergamon Press, Oxford, 1980.

[6] B. Radhakrishnan, R.G. Thompson, A model for formation and Solidification of Grain Boundary Liquid in the HAZ of Welds

[7] P. Pasquale, W. Pfeiffer, W. Burget, Numerical and experimental investigation on residual stresses in multi-run heavy section high strength welded joints, in: H. Cerjak (Ed.), Mathematical Modelling of Weld Phenomena 4, The Institute of Materials, Graz, Austria, 1998, pp. 620–630.

[8] D.E. Rodgers, P.R. Fletcher, The determination of internal stresses from the temperature history of a butt welded pipe, Weld. J. Res. Suppl. (1938) 4–7.

[9] D. Dye, O. Hunziker, R.C. Reed, Numerical analysis of the weldability of superalloys, Acta Mater. 49 (4) (2001) 683–697.

[10] D. Deng, Y. Luo, H. Serizawa, M. Shibahara, H. Murakawa, Numerical simulation of residual stress and deformation considering phase transformation effect, Trans. JWRI 32 (2003) 325–333.

[11] A. Godwin Antony, V. Vijayan, S. Saravanan, S. Baskar, M. Loganathan, Analysis of wear behaviour of aluminium composite with silicon carbide and titanium reinforcement, Int. J. Mech. Eng. Technol. 9 (2018) 681–691.

[12] S. Saravanan, A. Godwin Antony, V. Vijayan, M. Loganathan, S. Baskar, Synthesis of SiO2 nano particles by using sol-gel route, Int. J. Mech. Eng. Technol. 1 (2019) 785–790.

[13] S. Dinesh, A. Godwin Antony, K. Rajaguru, V. Vijayan, Experimental investigation and optimization of material removal rate and surface roughness in centerless grinding of magnesium alloy using grey relational analysis, Mech. Mech. Eng. 21 (2017) 17–28.

[14] S. Dinesh, K. Rajaguru, V. Vijayan, A. Godwin Antony, Investigation and prediction of material removal rate and surface roughness in CNC turning of EN24 alloy steel, Mech. Mech. Eng. , 20(2016), 451–466.

[15] B. Suresh Kumar, V. Vijayan, N. Baskar, Burr dimension analysis on various materials for convenantionally and CNC drilled holes, Mech. Mech. Eng. 20 (2016) 347–354.

[16] V.S. Shaisundaram, M. Chandrasekaran, S. Mohan Raj, R. Muraliraja, Investigation on the effect of thermal barrier coating at different dosing levels of cerium oxide nanoparticle fuel on diesel in a CI engine, Int. J. Ambient Energy 41 (1) (2020) 98–104.

[17] V.S. Shaisundaram, M. Chandrasekaran, M. Shanmugam, S. Padmanabhan, R. Muraliraja, L. Karikalan, (2019). Investigation of Momordica charantia seed biodiesel with cerium oxide nanoparticle on CI engine. Int. J. Ambient Energy, 1–5.

[18] V.S. Shaisundaram, M. Chandrasekaran, S. Mohan Raj, R. Muraliraja, T. Vinodkumar, Control of carbon dioxide emission in automobile vehicles using CO2 scrubber, Int. J. Ambient Energy 40 (7) (2019) 699–703.

[19] V.S. Shaisundaram, L. Karikalan, M. Chandrasekaran, (2019). Experimental investigation on the effect of cerium oxide nanoparticle fuel additives on pumpkin seed oil in CI engine, Int. J. Veh. Struct. Syst. (IJVSS), 11(3).

[20] R. Muraliraja, J. Sudagar, R. Elansezhian, A.V. Raviprakash, R. Dhinakaran, V.S. Shaisundaram, M. Chandrasekaran, Estimation of zwitterionic surfactant response in electroless composite coating and properties of Ni–P–CuO (nano)coating, Arab. J. Sci. Eng. 44 (2) (2019) 821–828.

[21] R. Arunachalam, K. Pradeep Kumar, R Muraliraja (2019). Optimization Of Stir-Squeeze Casting Parameters for Production of Metal Matrix Composites using A Hybrid Analytical Hierarchy Process-Taguchi Grey Approach, Engineering Optimization, Taylor and Francis.

[22] R. Muraliraja, R. Arunachalam, R. Ibrahim Al-Fori, Majid Al-Maharbi, Sujan Piya, (2019). Development of alumina reinforced aluminum metal matrix composite with enhanced compressive strength through squeeze casting process,J Materials: Design and Applications, SAGE Publication. (Impact factor 1.2).

[23] R. Muraliraja, R. Elansezhian, Influence of nickel recovery efficiency on crystallinity and microhardness of electroless Ni–P coatings and optimisation using Taguchi technique, Trans. IMF 93 (3) (2015) 126–132.

[24] R. Muraliraja, D. Sendilkumar, D.R. Elansezhian, Prediction and supplementation of reducing agent to improve the coating efficiency and wear behavior of electroless Ni-P plating, Int. J. Electrochem. Sci. 10 (2015) 5536–5547.

[25] Baskar Sanjeevi, Karikalan Loganathan, Synthesis of MWCNT nanofluid by using two step method, Therm. Sci. Int. Sci. J. (2019).

[26] S. Baskar, V. Vijayan, S. Saravanan, A.V. Balan, A. Godwin Antony, Effect of Al2O3, aluminium alloy and fly ash for making engine component, Int. J. Mech. Eng. Technol. (IJMET) 9 (12) (2018) 91–96.

[27] S. Baskar, L. Karikalan, V.S. Shai sundaram, S. Jacob, S. Venugopal, Theoretical study and performance of vapour refrigeration system along with additive of ZrO2, Int. J. Manage. Technol. Eng., ISSN NO: 2249-7455, 8(XII), 2018, 4811–4817.

[28] K. Jishuchandran, Manikandan, R. Ganesh, S. Baskar, Effect of nano-material on the performance patterns of waste cooking biodiesel fuelled diesel engine, Int. J. Ambient Energy, 1–16.

[29] D. Arunkumar, M. Ramu, R. Murugan, S. Kannan, S. Arun, Sanjeevi Baskar, Investigation of heat transfer of wall with and without using phase change material, Mater. Today: Proc., 1–5.

[30] K. Logesh, S. Baskar, M. Azeemudeen, B. Praveen Reddy, Gajavalli Venkata Subba Sai Jayanth, Analysis of cascade vapour refrigeration system with various refrigerants, Mater. Today: Proc. 18 (2019) 4659–4664.

Please cite this article as: S. Tamil Prabakaran, P. Sakthivel, M. Shanmugam et al., Modelling and experimental validation of TIG welding of INCONEL 718, Materials Today: Proceedings, https://doi.org/10.1016/j.matpr.2020.07.482